Dalton Transactions

RSC Publishing

PAPER

View Article Online
View Journal | View Issue

Open Access Article. Published on 16 May 2013. Downloaded on 12/29/2025 8:53:48 PM.
This article is licensed under a Creative Commons Attribution-NonCommercial 3.0 Unported Licence.

Cite this: *Dalton Trans.*, 2013, **42**, 10572

A comparative vibrational CD study of homo- and heteroleptic complexes of the type [Cu(*trans*-1,2-diaminocyclohexane)$_2$L](ClO$_4$)$_2$†

Christian Merten and Yunjie Xu*

Vibrational circular dichroism (VCD) spectroscopy is a powerful tool to characterize absolute configurations and conformations of chiral organometallic systems. Such characterizations rely on the corresponding density functional theory (DFT) spectral simulations which may become very time consuming and sometimes even impossible for systems with increasing complexity. Systematic studies on small model compounds can lead to empirical structure–spectra relationships. The present work continues the systematic investigations of transition metal complexes of chiral *trans*-1,2-diamino-cyclohexane (chxn). VA and VCD spectra of the mixed-ligand complexes $[Cu(chxn)_2L]^{2+}$ with L being either ethylene diamine (en) or *N*,*N*′-dimethylethylene diamine (dmen) are measured. The comparison of the experimental spectra of the mixed-ligand complexes with those of the distorted octahedral complex $[Cu(chxn)_3]^{2+}$ reveals that the VA and VCD patterns below 1500 cm^{-1} of the three complexes are not significantly affected by the nature of the third ligand, while the VCD pattern of the NH$_2$-bending modes in the 1500 to 1800 cm^{-1} region features some characteristic changes. Comparison with the corresponding DFT spectral calculations shows that these spectral differences are related to the relative abundance of the Δ- and Λ-configurations at the metal ion. In addition, the results of this study highlight that the VCD pattern of the NH$_2$-bending modes is characteristic of the coordination number and the configuration of the metal center.

Received 20th February 2013,
Accepted 15th May 2013

DOI: 10.1039/c3dt50459j

www.rsc.org/dalton

Introduction

Chiral organometallic compounds are being developed for a variety of applications. For instance, enantiopure transition metal catalysts such as Jacobson's catalysts were developed for the asymmetric epoxidation of alkenes,[1] and chiral metallocene based catalysts for isotactic olefin polymerisations.[2,3] Besides these single molecule catalysts, chiral metal–organic frameworks (MOFs) are of growing interest. This new class of hybrid materials features attractive possibilities to tune their structures and functions,[4–6] and chiral MOFs have been shown to be highly active asymmetric catalysts for various types of reactions.

Vibrational circular dichroism (VCD) spectroscopy, the vibrational counterpart of the well-known electronic circular dichroism spectroscopy, has been successfully used to characterize structures and chirality of a range of metal complexes. VCD studies of chiral metal complexes in general,[7–11] and of actual catalysts[12–14] and larger MOFs have been reported.[15–17] It is recognized that for larger molecules or complexes involving lanthanide ions, the corresponding theoretical spectral simulations can be extremely time consuming or even impossible at present time. Hence, it is desirable to study derivatives of smaller metal complexes systematically in order to derive some applicable structure–spectra relationships. In this context, Sato *et al.* investigated in detail the VCD spectra of tris (acetyl acetonate) complexes with different transition metal ions,[18] of their mixed ligand complexes,[19,20] and of larger multi-core complexes.[21–23]

Recently, we carried out a systematic study on the VCD spectra of transition metal complexes of copper(II) and nickel(II) with the chiral diamine ligands, *trans*-1,2-diamino cyclohexane (chxn).[24] It was shown that the obtained VCD spectra feature characteristic differences between the tris-complexes of Ni(II) and Cu(II), and between the tris- and bis-complexes of Cu(II). While the substitution of the metal ion caused intensity changes of specific bands, the change of the coordination number from 3 to 2 resulted in a sign inversion of the VCD couplet of the NH$_2$ bending vibration at ~1600 cm^{-1} and other changes in the VCD pattern.

Department of Chemistry, University of Alberta, Edmonton, Alberta T6G2G2, Canada. E-mail: yunjie.xu@ualberta.ca; Fax: +1 780 492 8231

†Electronic supplementary information (ESI) available: Selected structural parameters of $[Cu(chxn)_3]^{2+}$, various comparative plots, all calculated relative energy differences and single-conformer spectra, as well as the Cartesian coordinates for $[Cu(chxn)_3]^{2+}$. See DOI: 10.1039/c3dt50459j

This journal is © The Royal Society of Chemistry 2013

Open Access Article. Published on 16 May 2013. Downloaded on 12/29/2025 8:53:48 PM.
This article is licensed under a Creative Commons Attribution-NonCommercial 3.0 Unported Licence.

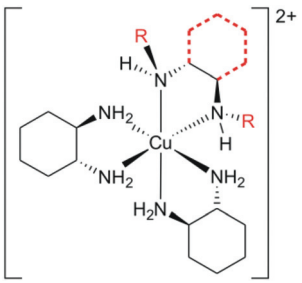

Fig. 1 Chemical structure of the Δ(λ)-isomer of $[Cu\{(R,R)\text{-chxn}\}_2(L)]^{2+}$. The substituted third (*R*,*R*)-chxn ligand is indicated in red dashed lines (R = H). For the mixed-ligand complexes with L = en (R = H) and L = dmen (R = CH_3), the dashed parts are not present.

In the present paper, we examine the associated VCD signatures when one chxn in $[Cu(chxn)_3](ClO_4)_2$ is replaced with ethylene diamine (en) or *N*,*N*′-dimethylethylene diamine (dmen) (Fig. 1). Both new ligands are achiral and are expected to contribute little to the experimental VA and VCD spectra on their own due to their relatively weak absorbance bands. This allows one to focus on the effects of the coordination number and the preference of Δ- and Λ-configurations of the metal ion on the VCD spectra upon ligand substitution. Hence, this study presents a first generalization of the previous findings on the relation between the observed experimental VCD spectra, in particular in the NH_2-bending region, and the configurations of the metal center. Interpretation of the experimental spectra is supported by density functional theory (DFT) based spectral calculations. For simplicity, the complexes with the (*R*,*R*)-enantiomer of chxn are always used when comparing experimental and calculated spectra.

Results and discussion

The tris(chxn) complex $[Cu(chxn)_3]^{2+}$

In order to compare the experimental and theoretical spectra as well as the conformational and energetic preferences of the studied mixed-ligand complexes with those of $[Cu(chxn)_3]^{2+}$, DFT calculations for this transition metal complex have been carried out which were not reported in the previous work.[24] The starting structures for the Δ- and Λ-isomers of $[Cu(chxn)_3]^{2+}$ were taken from those reported for $[Ni(chxn)_3]^{2+}$.[24] During the geometry optimizations, the point group has been reduced to C_2 due to Jahn–Teller distortion of the octahedral d^9 system.[25] This is consistent with the crystal structure of $[Cu(chxn)_3](ClO_4)_2$ which also features a C_2 symmetry.[26] Some structural parameters obtained from the calculations are summarized in the ESI.† Based on the calculated relative energy differences, the Λ-isomer is favoured by ΔE_{GP} = 0.13 kcal mol^{-1} and ΔG_{GP} = 0.41 kcal mol^{-1} where GP stands for gas phase. The corresponding Boltzmann populations at 298 K are 55.3% and 44.7% with respect to ΔE_{GP}, and 66.6% and 33.4% for ΔG_{GP}. In order to evaluate possible effects of the solvent environment on the VCD pattern, the geometry optimizations and spectra calculations have been repeated using the integral equation formalism (IEF) version of the polarizable continuum model (PCM) of DMSO,[27,28] resulting in a preference of the Δ-isomer by ΔE_{PCM} = 0.46 kcal mol^{-1} and ΔG_{PCM} = 1.22 kcal mol^{-1}.

The gas phase ΔE and ΔG based population weighted VA and VCD spectra are quite similar, except for the intensity variations of the NH_2-bending modes (*cf.* Fig. S2†). The same can be said about the corresponding IEFPCM spectra. Fig. 2 shows a comparison of the experimental VA and VCD spectra of $[Cu(chxn)_3](ClO_4)_2$ with the ΔE_{GP} and ΔE_{PCM} weighted spectra in the gas phase and with IEFPCM, respectively. First, comparing the experimental and the gas phase spectra, the main features of the experimental spectra are found to be reproduced theoretically. On the other hand, some deviations in the VCD spectral pattern in the 1375–1300 cm^{-1} region are observed. In addition, the medium intensity VCD band observed at 1200 cm^{-1} is predicted to have almost no VCD intensity at around 1178 cm^{-1}. The corresponding VA band observed experimentally is predicted to be very weak. Similar deviations were noted with the gas phase calculations for $[Ni(chxn)_3]^{2+}$ in the previous study.[24] Second, comparing the gas phase with the IEFPCM spectra, the VA bands and the VCD couplet of the NH_2-bending modes at 1600 cm^{-1} are predicted to be much more intense in the IEFPCM calculations. Considering the experimental intensity ratio of the large (+) and the small (−) components of the couplet being ~2, the IEFPCM calculation describes the VCD spectral features of the NH_2-bending modes significantly better than the gas phase one. The experimental VCD pattern in the range from 1380–1300 cm^{-1} is also better described by the IEFPCM calculation, although the negative VCD shoulder band observed at 1380 cm^{-1} is predicted as a positive band at 1371 cm^{-1}. Furthermore, both VA and VCD

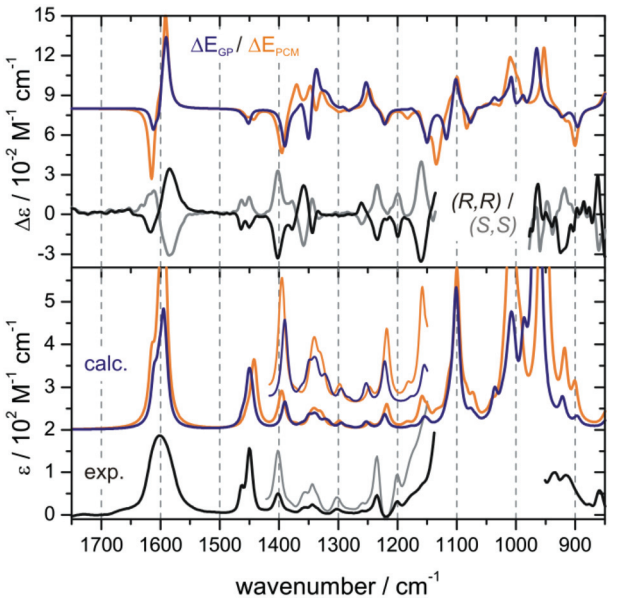

Fig. 2 Comparison of the experimental VA and VCD spectra of $[Cu(chxn)_3](ClO_4)_2$ with the calculated spectra. Both ΔE_{GP} (blue) and ΔE_{PCM} (orange) population weighted spectra are shown.

Open Access Article. Published on 16 May 2013. Downloaded on 12/29/2025 8:53:48 PM.
This article is licensed under a Creative Commons Attribution-NonCommercial 3.0 Unported Licence.

bands observed at 1200 cm^{-1} are reasonably predicted with IEFPCM. Overall, the IEFPCM based spectra agree qualitatively better with the experiment than the gas phase ones. The better agreement in the region below 1500 cm^{-1} is due to the somewhat different VCD patterns generated in the gas phase and in the IEFPCM solution, rather than the changes in the relative population weights of different isomers. This statement is supported by the comparison of the single-isomer spectra (Fig. S3†) generated by the gas phase and IEFPCM calculations.

The mixed-ligand complex $[Cu(chxn)_2(en)]^{2+}$

The experimentally obtained VA and VCD spectra of both enantiomers of $[Cu(chxn)_2(en)](ClO_4)_2$ are shown in Fig. 3. When compared to $[Cu(chxn)_3](ClO_4)_2$, the VCD spectral pattern is found to be very similar. Differences in the absolute intensities of the bands can be mostly related to the decreased number of chiral chxn ligands which contribute to these bands (see Fig. S4† for a direct comparison of the experimental VCD spectra of the tris(chxn) and mixed-ligand complexes studied).

In the tris(chxn) complexes, the structure and chirality of the chxn ligand hold the NCCN torsional angle in a fixed conformation. The NCCN angle is negative for the (*R*,*R*)-enantiomer of chxn, which is also referred to as the λ-conformation. In $[Cu(chxn)_2(en)]^{2+}$, the en ligand is flexible and can adopt in general either the δ- or λ-conformation. This generates four possible isomers, Δ(δ-en), Δ(λ-en), Λ(δ-en), and Λ(λ-en). Furthermore, the new ligand en can bind in two different ways to the copper center: it can either occupy two equatorial positions leaving the axial positions to the nitrogen atoms of the two chxn groups, or it can place one of its nitrogen atoms on an axial position. While the first set of conformers all belong to the C_2 point group, the latter set is of C_1-symmetry. Hence, for the $[Cu(chxn)_2(en)]^{2+}$ complex, a total of 8 conformations has to be considered. The relative energy differences Δ*E* for the eight conformations calculated in the gas phase and using the IEFPCM of DMSO are summarized in Table 1, whereas the related Δ*G* values and populations can be found in Table S2 of the ESI.† The calculated relative energies indicate a clear preference for the C_1-symmetric structures with the smaller and more flexible en ligand occupying an axial position. The structures of the four C_1-conformers with en on the axial positions are shown in Fig. 4. The conformation of the en ligand does not significantly affect the geometry of the remaining part of the complex, as can be seen when one superimposes the calculated structures in Fig. S5 of the ESI.†

Table 1 Relative energies Δ*E* (in kcal mol^{-1}) and the corresponding percentage Boltzmann population factors at room temperature of the eight calculated conformers of $[Cu(chxn)_2(en)]^{2+}$ in the gas phase and in solution using the IEFPCM for DMSO. In the C_1-conformers, en occupies one axial and one equatorial position, while it occupies two equatorial positions in the C_2-conformers

Conf.	en	ΔE_{GP} (kcal mol^{-1})	pop-ΔE_{GP} (%)	ΔE_{PCM} (kcal mol^{-1})	pop-ΔE_{PCM} (%)
Λ(δ-en) C_1	ax	0.00	31.05	0.27	17.14
Λ(δ-en) C_2	eq	1.74	1.65	1.52	2.06
Δ(δ-en) C_1	ax	0.06	28.25	0.00	26.86
Δ(δ-en) C_2	eq	1.74	1.64	0.37	14.37
Δ(λ-en) C_1	ax	0.30	18.79	0.15	20.89
Δ(λ-en) C_2	eq	2.12	0.86	0.99	5.09
Λ(λ-en) C_1	ax	0.37	16.63	0.53	11.05
Λ(λ-en) C_2	eq	1.96	1.13	1.39	2.55

Since the Δ*G* (not shown) and Δ*E* weighted spectra are essentially identical, only the ΔE_{GP} and ΔE_{PCM} population weighted VA and VCD spectra are compared to the experimental spectra in Fig. 3. Both sets of simulations predict the main experimental VCD spectral features such as the couplet of the NH_2-bending mode correctly. It is noted that the gas phase VCD pattern predicted for the mixed-ligand complex in the 1400–1200 cm^{-1} region is essentially the same as for $[Cu(chxn)_3]^{2+}$, although with an overall reduction in intensity. The

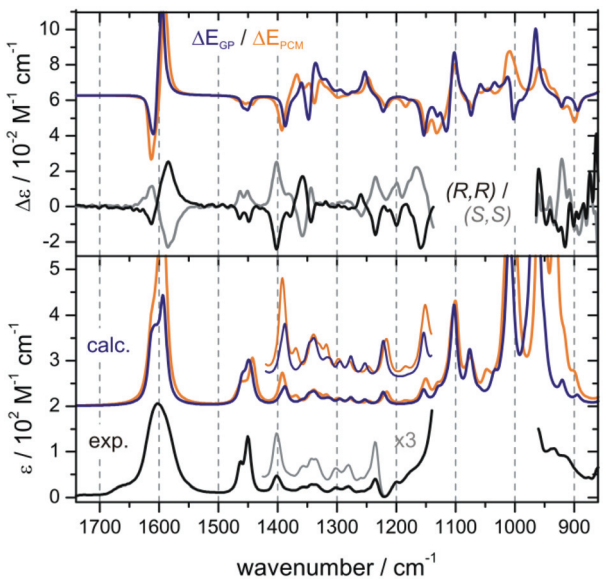

Fig. 3 Comparison of the experimental VA and VCD spectra of $[Cu(chxn)_2(en)]^{2+}$ with the calculated spectra. Both ΔE_{GP} (blue) and ΔE_{PCM} (orange) population weighted spectra are shown.

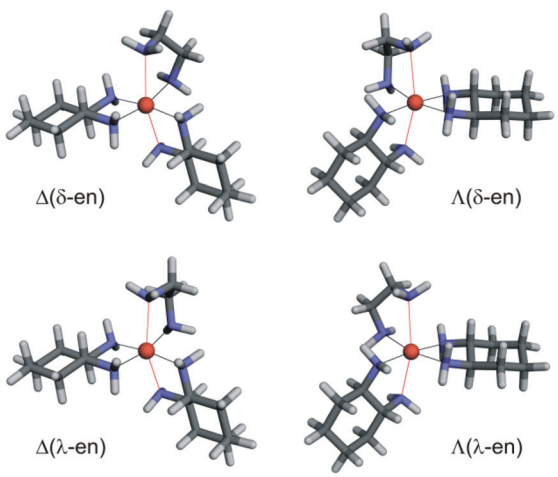

Fig. 4 Optimized geometries of the four C_1(en-ax) isomers of $[Cu(chxn)_2(en)]^{2+}$. The axial bonds are highlighted in red. The associated Cartesian coordinates are provided in the ESI.†

This journal is © The Royal Society of Chemistry 2013

Open Access Article. Published on 16 May 2013. Downloaded on 12/29/2025 8:53:48 PM.
This article is licensed under a Creative Commons Attribution-NonCommercial 3.0 Unported Licence.

same observation can be made about the IEFPCM spectra. It is therefore not surprising that the same discrepancies between experimental and theoretical spectra noted for the tris(chxn) complex persist for the mixed-ligand complex here.

The mixed-ligand complex $[Cu(chxn)_2(dmen)]^{2+}$

In the second mixed-ligand complex of this study, dimethyl ethylenediamine (dmen) is binding to the bis(chxn) complex yielding $[Cu(chxn)_2(dmen)](ClO_4)_2$. The experimental VA and VCD spectra for both enantiomers of this complex are shown in Fig. 5. The observed VCD pattern is very similar to that of $[Cu(chxn)_2(en)]^{2+}$ shown previously. Furthermore, the VCD intensities in the range below 1500 cm^{-1} are also almost the same for the two mix-ligand complexes. The intensity of the NH_2-bending modes, on the other hand, is significantly decreased in both VA and VCD spectra, as it can be expected from the substitution of the two hydrogen atoms with the two methyl groups. The VA spectrum also becomes broadened in the range from 1500–1400 cm^{-1} because of the additional bending modes of the methyl groups. This broadening did not affect the VCD pattern or the VCD intensity of the bands, though.

For the calculations on $[Cu(chxn)_2(dmen)]^{2+}$, the same eight diastereomeric configurations Δ(δ-dmen), Δ(λ-dmen), Λ(δ-dmen), and Λ(λ-dmen) with dmen being in an axial or equatorial position have to be considered. Additionally, the introduction of the methyl groups on each of the amino groups further increases the number of possible conformations for each of these eight configurations. By systematically substituting hydrogen atoms of the amino groups with methyl groups, four different conformations for each diastereomeric configuration can be generated. Two of them have the methyl groups bound in *trans* conformations, two in a *cis* conformation (*cf.* Fig. 6). When dmen binds to the metal center in the equatorial positions, only one *cis* conformer is obtained due to symmetry. Hence, in total, 28 conformers of $[Cu(chxn)_2(dmen)]^{2+}$ can be generated. Since no noticeable differences have been observed for the gas phase and the IEFPCM simulated VA and VCD spectra for the two complexes discussed above, only the gas phase calculations have been carried out for this third complex. The relative energies and Gibbs free energies, ΔE_{GP} and ΔG_{GP}, as well as the corresponding Boltzmann populations are summarized in Table 2.

Due to the large number of conformers, it is more complicated to evaluate which conformations are preferably adopted.

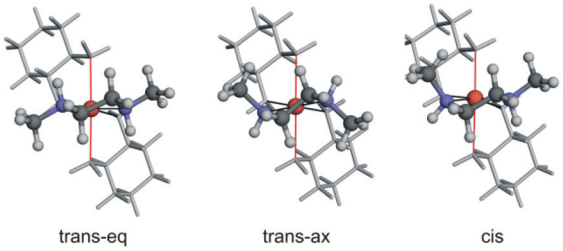

Fig. 6 Three binding configurations of the methyl groups of dmen in $[Cu(chxn)_2(dmen)]^{2+}$ shown along the N–Cu–N plane of the dmen-ligand exemplified for the C_2-symmetric Δ(λ-dmen) isomer. The axial Cu–N bonds are highlighted in red and the nitrogen atoms of dmen are placed in the equatorial positions of the octahedral ligand sphere. The methyl groups of dmen can either be equatorial or axial with respect to the N–Cu–N plane (*trans*-eq and *trans*-ax conformer), or they are located in a *cis* type conformation.

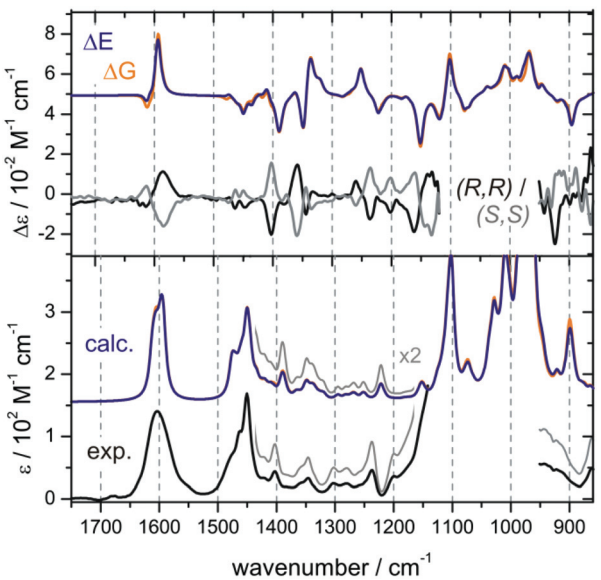

Fig. 5 Comparison of the experimental VA and VCD spectra of $[Cu(chxn)_2(dmen)]^{2+}$ with the calculated spectra. Both ΔE_{GP} (blue) and ΔG_{GP} (orange) population weighted spectra are shown.

Table 2 Relative energies ΔE_{GP} and Gibbs free energies ΔG_{GP} (in kcal mol^{-1}), as well as the corresponding percentage Boltzmann population factors of the 28 conformers of $[Cu(chxn)_2(dmen)]^{2+}$. The column dmen shows whether the achiral ligand is in the axial or equatorial position

Conf.		dmen	ΔE	ΔG	pop-ΔE	pop-ΔG
Λ(δ-dmen)	*trans*-eq	ax	0.00	0.00	29.02	28.84
Λ(δ-dmen)	*trans*-ax	ax	3.21	3.56	0.13	0.07
Λ(δ-dmen)	*cis*1	ax	2.26	2.55	0.63	0.39
Λ(δ-dmen)	*cis*2	ax	1.13	1.37	4.33	2.86
Λ(δ-dmen)	*trans*-ax	eq	3.86	4.79	0.04	0.01
Λ(δ-dmen)	*trans*-eq	eq	0.90	1.48	6.31	2.35
Λ(δ-dmen)	*cis*	eq	1.84	1.96	1.29	1.06
Δ(λ-dmen)	*trans*-eq	ax	0.39	0.05	14.95	26.30
Δ(λ-dmen)	*trans*-ax	ax	2.63	2.72	0.34	0.29
Δ(λ-dmen)	*cis*1	ax	1.32	1.23	3.13	3.59
Δ(λ-dmen)	*cis*2	ax	1.77	1.61	1.47	1.91
Δ(λ-dmen)	*trans*-ax	eq	4.20	4.75	0.02	0.01
Δ(λ-dmen)	*trans*-eq	eq	0.77	0.79	7.96	7.56
Δ(λ-dmen)	*cis*	eq	2.28	2.59	0.62	0.36
Δ(δ-dmen)	*trans*-ax	ax	0.97	1.23	5.63	3.64
Δ(δ-dmen)	*trans*-eq	ax	1.56	1.44	2.09	2.51
Δ(δ-dmen)	*cis*1	ax	1.16	1.11	4.09	4.44
Δ(δ-dmen)	*cis*2	ax	1.18	0.95	3.93	5.82
Δ(δ-dmen)	*trans*-ax	eq	1.99	2.31	1.00	0.58
Δ(δ-dmen)	*trans*-eq	eq	2.10	2.80	0.84	0.26
Δ(δ-dmen)	*cis*	eq	2.13	2.65	0.79	0.33
Λ(λ-dmen)	*trans*-ax	ax	1.60	1.75	1.94	1.49
Λ(λ-dmen)	*trans*-eq	ax	1.70	1.75	1.65	1.51
Λ(λ-dmen)	*cis*1	ax	2.20	2.60	0.71	0.36
Λ(λ-dmen)	*cis*2	ax	1.48	1.84	2.37	1.29
Λ(λ-dmen)	*trans*-ax	eq	1.42	1.71	2.65	1.61
Λ(λ-dmen)	*trans*-eq	eq	1.92	2.77	1.13	0.27
Λ(λ-dmen)	*cis*	eq	2.04	2.71	0.93	0.30

Open Access Article. Published on 16 May 2013. Downloaded on 12/29/2025 8:53:48 PM.
This article is licensed under a Creative Commons Attribution-NonCommercial 3.0 Unported Licence.

Nevertheless, the Boltzmann factors tabulated in Table 2 clearly show that the *trans*-eq forms of the Λ(δ-dmen) and Δ(λ-dmen) isomers with dmen occupying the axial position in the complex have by far the largest contribution to the conformational equilibrium of $[Cu(chxn)_2(dmen)]^{2+}$. The preference of these two configurations could be understood by considering steric hindrance caused by the two methyl groups. Such repulsive energy is at the lowest in the *trans*-eq conformation when more space is available for the methyl groups (*cf.* Fig. 6).

The theoretical spectra shown in Fig. 5 are obtained by using the population factors listed in Table 2. No significant differences between the ΔE_{GP} and ΔG_{GP} weighted spectra of $[Cu(chxn)_2(dmen)]^{2+}$ are observed. Despite the existence of a large number of relevant conformers, reasonably good agreement between the simulated and experimental spectra has been achieved for this complex, as for the other two complexes discussed above. It is worth pointing out that the significantly lower intensity of the negative part of the couplet of the NH_2-bending modes observed experimentally is well captured by the simulation. The considerable intensity decrease observed for the VCD bands below 1300 cm^{-1} is also well reproduced by the current simulation.

Comparison of the three complexes

First, the effects of the substituted ligands, *i.e.* en and dmen, on the theoretical VCD spectrum of each individual conformer are examined. Fig. 7 shows the theoretical VCD spectra of the two conformers of $[Cu(chxn)_3]^{2+}$ and of the eight conformers of $[Cu(chxn)_2(en)]^{2+}$ as obtained from the IEFPCM calculations. The gas phase single conformer spectra of $[Cu(chxn)_2(dmen)]^{2+}$ are shown in Fig. S6 of the ESI.† In Fig. 7, the spectra of $[Cu(chxn)_2(en)]^{2+}$ are grouped by the δ- and λ-conformations of the en ligand to allow a direct comparison of the Δ- and Λ-configurations of the metal ion.

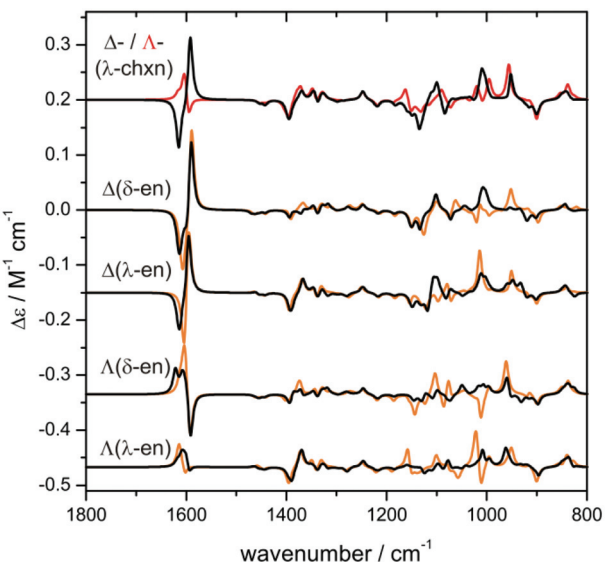

Fig. 7 Comparison of the single isomer spectra of $Cu(chxn)_3^{2+}$ (top trace) and the en-ax (black) and en-eq (orange) isomers of $Cu(chxn)_2(en)^{2+}$.

The NH_2-bending modes centred at 1600 cm^{-1} are highly sensitive to the Δ- and Λ-configurations of the metal ion. The third ligand substitution introduces additional sensitivity to the δ- and λ-configurations of the en ligand, especially when the metal ion is in the Λ-configuration and, to a lesser degree, to whether the third ligand occupies the axial or equatorial positions. Specifically, the Δ-isomers all show a −/+ pattern while the Λ-isomers show an all-positive pattern in the case of the Λ(λ-en) isomer and a +/− pattern for the Λ(δ-en) isomer. The next region from 1500 cm^{-1} to 1200 cm^{-1} shows *only* sensitivity to whether the third ligand, en, is in the δ- or λ-configuration. This means that the VCD features in this region remain essentially unchanged for Δ(λ-chxn) and Λ(λ-chxn), and for Δ(λ-en) and Λ(λ-en), with en in either the axial or equatorial position, whereas those associated with (δ-en) appear differently. In the region below 1300 cm^{-1}, which is covered by strong bands from the solvent and the anion in the experiment, the VCD pattern is sensitive to the configuration of the metal ion and the conformation of the third ligand, as well as the binding site occupied by the third ligand. Closer examination in this region reveals another characteristic feature for the Δ-isomers with a more intense negative band at 1150 cm^{-1} than the Λ-isomers. Similar conclusions can also be drawn from the gas phase spectra of the above complexes (Fig. S6†).

Since these metal complexes contain multiple relevant conformers, the relative abundance of them is also important for the comparison between theoretical and experimental spectra. Table 3 summarizes the calculated populations of the Δ- and Λ-isomers of the three investigated complexes based on the ΔE and ΔG values. While the ΔE based gas phase populations suggest that the Δ- and Λ-forms of the complexes studied are of more or less the same stability, the ΔG_{GP} populations, however, show a switch of preference from the Δ- to the Λ-form upon third ligand substitution. The ΔE and ΔG values obtained with the IEFPCM calculations show a clear preference for the Δ- over the Λ-form for the two complexes calculated. This switch of conformational preferences depending on the choice of ΔE or ΔG for its calculation has been observed before.[29,30]

As pointed out before, the spectral patterns of the experimental VA and VCD spectra of all three complexes appear fairly similar. The main differences observed are the overall VCD intensity for each complex and the relative intensity of the couplet of the NH_2 bending modes (see Fig. S4†). In the case of the $[Cu(chxn)_2(dmen)]^{2+}$ complex, changes are also noted for the VA intensities of some bands. The first and the last observations can be directly related to the number of chiral chxn ligands in the complex and to the substitution of two NH_2-groups by $NHCH_3$-groups in dmen, respectively. The interpretation for the relative intensity of the couplet of the NH_2 bending modes is somewhat more involved. As discussed before, while Δ-conformers show −/+ couplets with similar strong intensity, Λ-conformers exhibit roughly +/− couplets with lower intensity. Hence, the intensity ratio of the two components of the couplet is a characteristic for the relative population of the Δ- and Λ-conformers. For example, by

 This journal is © The Royal Society of Chemistry 2013

Open Access Article. Published on 16 May 2013. Downloaded on 12/29/2025 8:53:48 PM.
This article is licensed under a Creative Commons Attribution-NonCommercial 3.0 Unported Licence.

Table 3 Summary of the calculated populations of the Δ- and Λ-conformers of $[CuL_3]^{2+}$, $[CuL_2en]^{2+}$, and $[CuL_2dmen]^{2+}$ with L = chxn

	pop-ΔE_{GP}		pop-ΔG_{GP}		pop-ΔE_{PCM}		pop-ΔG_{PCM}	
	Σ(Δ)	Σ(Λ)	Σ(Δ)	Σ(Λ)	Σ(Δ)	Σ(Λ)	Σ(Δ)	Σ(Λ)
$[CuL_3]^{2+}$	44.7	55.3	33.4	66.6	68.5	31.5	88.7	11.3
$[CuL_2en]^{2+}$	49.5	50.5	62.0	38.0	67.2	32.8	84.6	15.4
$[CuL_2dmen]^{2+}$	46.9	53.1	57.6	42.4	—[a]	—	—	—

[a] IEFPCM calculations were not carried out for $[Cu(chxn)_2dmen]^{2+}$. See the main text for the discussion.

varying the ratio of the Δ- and Λ-forms of the presented theoretical spectra, the NH_2-bending modes of $[Cu(chxn)_3]^{2+}$ would become all positive when one assumes a conformational distribution of 25% Δ- and 75% Λ-conformers. Generally, the Δ-form can be regarded as the dominating form in all three investigated complexes since the −/+ pattern is preserved.

As reported previously, the change of the coordination number from 3 to 2 resulted in a sign inversion of the VCD couplet of the NH_2 bending vibration modes at ~1600 cm^{-1} from the tris- to bis-complexes of $[Cu(chxn)_{2,3}]^{2+}$.[24] The current comparative study with both the homoleptic tris-complex $[Cu(chxn)_3]^{2+}$ and the mixed-ligand complexes, $[Cu(chxn)_2(en)]^{2+}$ and $[Cu(chxn)_2(dmen)]^{2+}$, further confirms that such sign change is characteristic of the coordination number of all ligands, rather than the total number of chiral ligands.

Conclusions

In summary, VA and VCD spectra of the distorted octahedral complex $[Cu(chxn)_3]^{2+}$ and the mixed-ligand complexes $[Cu(chxn)_2(en)]^{2+}$ and $[Cu(chxn)_2(dmen)]^{2+}$ have been measured and their corresponding theoretical spectra have been calculated. The comparison of the experimental spectra reveals that the VA and VCD patterns below 1500 cm^{-1} of the three complexes are not significantly affected by the nature of the third ligand, while the VCD pattern above 1500 cm^{-1} exhibits some characteristic changes.

Considering the results of the calculations, several conclusions can be drawn. First of all, the calculated spectra agree reasonably well with the corresponding experimental data. Second, the signs of the VCD couplet of the NH_2-bending modes are characteristic of the coordination number of the ligands around the metal ion for the homo- and heteroleptic complexes studied. Third, the Δ- and Λ-configurations each feature a distinct VCD pattern at the NH_2-bending modes, and the ratio of the (−) and (+) components of the doublet is related to the relative abundance of the Δ- and Λ-forms. In all three investigated complexes, the dominant configuration of the metal center is Δ. Fourth, the cause of the less satisfying agreement between experiment and theory in the 1400–1300 cm^{-1} region is unclear. Further studies of the related deuterated species and the mixed-ligand complexes of $[Cu(chxn)_2]^{2+}$ with larger achiral and also chiral diamine ligands are planned in order to shed light on this disagreement. A good understanding of the cause is crucial for a reliable VCD spectral interpretation of chiral metal complexes and even larger metal organic networks.

Experimental and computational methods

Materials

All chemicals were purchased from Sigma Aldrich and were used without further purification. The bis- and tri-chelates have been synthesized by mixing the corresponding metal perchlorate salts with the respective equivalents of enantiopure chxn in methanol.[24] The corresponding elemental analysis is given in ref. 24. For the spectroscopic study, the mixed-ligand complexes have been generated *in situ* by dissolving equimolar amounts of $[Cu(chxn)_2](ClO_4)_2$ and the third respective ligand in DMSO-d_6.

VA and VCD spectroscopy

The VA and VCD spectra have been recorded in the fingerprint region (1800–850 cm^{-1}) with a Bruker Vertex 70 FT-IR spectrometer equipped with a Bruker PMA 50 module for VCD measurements. The samples were held in a demountable BaF_2 cell with a pathlength of 100 μm. For the VCD spectra, a minimum of 20 000 scans have been averaged. The concentrations of the metal complexes in DMSO-d_6 were 100 mg ml^{-1}. The region from 1140 to 950 cm^{-1} has been cut out in all experimental spectra due to interference of the absorbance bands of the solvent and the perchlorate ion.

Computational details

Geometry optimizations and harmonic calculations of vibrational frequencies of all conformers as well as VA and VCD spectra calculations have been performed in the DFT framework at the B3LYP/6-311++G(2d,p) level of theory using Gaussian 09 C.01.[31] The zero-point-corrected energies and the related free energies at 298 K of all conformers are compared. The relative ΔE value of the most stable conformer is set to zero as the reference point for the other conformers. The same procedure was applied to the ΔG values. The Boltzmann population factors at room temperature have been calculated based on these relative energies. All calculations have been performed for the (*R*,*R*)-enantiomers in the gas phase. For $[Cu(chxn)_3]^{2+}$ and $[Cu(chxn)_2(en)]^{2+}$, solvent effects have been accounted for by using the integral equation formalism (IEF) version of the polarizable continuum model (PCM) for DMSO.[27,28] The counterions do not affect the VCD spectral

Open Access Article. Published on 16 May 2013. Downloaded on 12/29/2025 8:53:48 PM.
This article is licensed under a Creative Commons Attribution-NonCommercial 3.0 Unported Licence.

features in these complexes. This was demonstrated for the VCD spectrum of the $[Ni(chxn)_3]^{2+}$ complex which showed no changes when different counterions were implemented.[24] Therefore, we have not included the counterions in the simulations. Solution line broadening has been taken into account by assigning a Lorentzian band shape with a half-width at half-height of 6 cm^{-1}. The calculated wavenumbers have been scaled by 0.97 for better visual comparison with the experimental data.

Acknowledgements

This research was funded by the University of Alberta and the Natural Sciences and Engineering Research Council of Canada. We also gratefully acknowledge access to the computing facilities provided by the Western Canada Research Grid (Westgrid) and Sharcnet. CM thanks the Alexander von Humboldt Foundation for a Feodor Lynen Postdoctoral Fellowship. YX holds a Tier I (Senior) Canada Research Chair in Chirality and Chirality Recognition.

Notes and references

1 S. E. Reisman, A. G. Doyle and E. N. Jacobsen, *J. Am. Chem. Soc.*, 2008, **130**, 7198–7199.
2 Y. Nakayama and T. Shiono, *Molecules*, 2005, **10**, 620–633.
3 H. H. Brintzinger, D. Fischer, R. Mülhaupt, B. Rieger and R. M. Waymouth, *Angew. Chem., Int. Ed. Engl.*, 1995, **34**, 1143–1170.
4 G. Nickerl, A. Henschel, R. Grünker, K. Gedrich and S. Kaskel, *Chem. Ing. Tech.*, 2011, **83**, 90–103.
5 L. Ma, J. M. Falkowski, C. Abney and W. Lin, *Nat. Chem.*, 2010, **2**, 838–846.
6 Y. Liu, W. Xuan and Y. Cui, *Adv. Mater.*, 2010, **22**, 4112–4135.
7 P. J. Stephens, F. J. Devlin, C. Villani, F. Gasparrini and S. L. Mortera, *Inorg. Chim. Acta*, 2008, **361**, 987–999.
8 D. A. Young, T. B. Freedman, E. D. Lipp and L. A. Nafie, *J. Am. Chem. Soc.*, 1986, **108**, 7255–7263.
9 T. B. Freedman, X. Cao, D. A. Young and L. A. Nafie, *J. Phys. Chem. A*, 2002, **106**, 3560–3565.
10 P. R. Lassen, L. Guy, I. Karame, T. Roisnel, N. Vanthuyne, C. Roussel, X. Cao, R. Lombardi, J. Crassous, T. B. Freedman and L. A. Nafie, *Inorg. Chem.*, 2006, **45**, 10230–10239.
11 A.-C. Chamayou, S. Lüdeke, V. Brecht, T. B. Freedman, L. A. Nafie and C. Janiak, *Inorg. Chem.*, 2011, **50**, 11363–11374.
12 C. Merten, M. Amkreutz and A. Hartwig, *J. Mol. Struct.*, 2010, **970**, 101–105.
13 C. Johannessen, L. Hecht and C. Merten, *ChemPhysChem*, 2011, **12**, 1419–1421.
14 Z. Dezhahang, C. Merten, M. R. Poopari and Y. Xu, *Dalton Trans.*, 2012, **41**, 10817–10824.
15 Z.-B. Han, J.-W. Ji, H.-Y. An, W. Zhang, G.-X. Han, G.-X. Zhang and L.-G. Yang, *Dalton Trans.*, 2009, 9807–9811.
16 C. Jahier, M. Cantuel, N. D. McClenaghan, T. Buffeteau, D. Cavagnat, F. Agbossou, M. Carraro, M. Bonchio and S. Nlate, *Chem.–Eur. J.*, 2009, **15**, 8703–8708.
17 D. W. Armstrong, F. A. Cotton, A. G. Petrovic, P. L. Polavarapu and M. M. Warnke, *Inorg. Chem.*, 2007, **46**, 1535–1537.
18 H. Sato, T. Taniguchi, A. Nakahashi, K. Monde and A. Yamagishi, *Inorg. Chem.*, 2007, **46**, 6755–6766.
19 H. Sato, Y. Mori, Y. Fukuda and A. Yamagishi, *Inorg. Chem.*, 2009, **48**, 4354–4361.
20 H. Sato, H. Uno and H. Nakano, *Dalton Trans.*, 2011, **40**, 1332–1337.
21 H. Sato, R. Takase, Y. Mori and A. Yamagishi, *Dalton Trans.*, 2011, **41**, 747–751.
22 H. Sato, F. Sato, M. Taniguchi and A. Yamagishi, *Dalton Trans.*, 2012, **41**, 1709–1712.
23 H. Sato and A. Yamagishi, *Int. J. Mol. Sci.*, 2013, **14**, 964–978.
24 C. Merten, K. Hiller and Y. Xu, *Phys. Chem. Chem. Phys.*, 2012, **14**, 12884–12891.
25 J. K. Burdett, *Inorg. Chem.*, 1981, **20**, 1959–1962.
26 C. Pariya, K. Panneerselvan, C.-S. Chung and T.-H. Lub, *Polyhedron*, 1998, **17**, 2555–2561.
27 J. Tomasi, B. Mennucci and R. Cammi, *Chem. Rev.*, 2005, **105**, 2999–3094.
28 B. Mennucci, C. Cappelli, R. Cammi and J. Tomasi, *Chirality*, 2011, **23**, 717–729.
29 G. Longhi, S. L. Fornili, V. T. Liveri, S. Abbate, D. Rebeccani, L. Ceraulo and F. Gangemi, *Phys. Chem. Chem. Phys.*, 2010, **12**, 4694–4703.
30 D. J. Miller and J. M. Lisy, *J. Am. Chem. Soc.*, 2008, **130**, 15393–15404.
31 M. J. Frisch, G. W. Trucks, H. B. Schlegel, G. E. Scuseria, M. A. Robb, J. R. Cheeseman, G. Scalmani, V. Barone, B. Mennucci, G. A. Petersson, H. Nakatsuji, M. Caricato, X. Li, H. P. Hratchian, A. F. Izmaylov, J. Bloino, G. Zheng, J. L. Sonnenberg, M. Hada, M. Ehara, K. Toyota, R. Fukuda, J. Hasegawa, M. Ishida, T. Nakajima, Y. Honda, O. Kitao, H. Nakai, T. Vreven, J. J. A. Montgomery, J. E. Peralta, F. Ogliaro, M. Bearpark, J. J. Heyd, E. Brothers, K. N. Kudin, V. N. Staroverov, T. Keith, R. Kobayashi, J. Normand, K. Raghavachari, A. Rendell, J. C. Burant, S. S. Iyengar, J. Tomasi, M. Cossi, N. Rega, J. M. Millam, M. Klene, J. E. Knox, J. B. Cross, V. Bakken, C. Adamo, J. Jaramillo, R. Gomperts, R. E. Stratmann, O. Yazyev, A. J. Austin, R. Cammi, C. Pomelli, J. W. Ochterski, R. L. Martin, K. Morokuma, V. G. Zakrzewski, G. A. Voth, P. Salvador, J. J. Dannenberg, S. Dapprich, A. D. Daniels, O. Farkas, J. B. Foresman, J. V. Ortiz, J. Cioslowski and D. J. Fox, *GAUSSIAN 09 (Revision C.01)*, Gaussian, Inc., Wallingford, CT, 2010.

 This journal is © The Royal Society of Chemistry 2013